Nanoscale Advances

ROYAL SOCIETY OF CHEMISTRY

PAPER

View Article Online
View Journal | View Issue

Cite this: *Nanoscale Adv.*, 2021, **3**, 2030

Tight-binding investigation of the structural and vibrational properties of graphene–single wall carbon nanotube junctions†

Juhi Srivastava[ab] and Anshu Gaur *[ab]

Hybrid carbon nanostructures based on single walled carbon nanotubes (SWNTs) and single layer graphene (SLG) have drawn much attention lately for their applications in a range of efficient hybrid devices. A few recent studies, addressing the interaction behavior at the heterojunction, considered charge transfer between the constituents (SWNTs and SLG) to be responsible for changes in the electronic and vibrational properties of their hybrid system. We report the effect of various factors, arising due to the interactions between the atoms of SWNTs and SLG, on the structural and vibrational properties of hybrid nanostructures investigated computationally within the framework of tight-binding DFT. These factors, such as the van der Waals (vdW) forces, structural deformation and charge transfer, are seen to affect the Raman active phonon frequencies of SWNTs and SLG in the hybrid nanostructure. These factors are already known to affect the vibrational properties of SWNTs and SLG separately and in this work, we have explored their role and interplay between these factors in hybrid systems. The contribution of different factors to the total shift observed in phonon frequencies is estimated and it is perceived from our findings that not only the charge transfer but the structural deformations and the vdW forces also affect the vibrational properties of components within the hybrid, with structural deformation being the leading factor. With decreasing separation between SWNTs and SLG, the charge transfer and the vdW forces both increase. However, the increase in vdW forces is relatively much higher and likely to be the main cause for larger Raman shifts observed at smaller separations.

Received 21st October 2020
Accepted 5th February 2021

DOI: 10.1039/d0na00881h

rsc.li/nanoscale-advances

1 Introduction

Nano-sized carbon allotropes, specially single-walled carbon nanotubes (SWNTs) and single-layer graphene (SLG), are the most widely studied materials due to their extraordinary mechanical, chemical and optical properties[1–6] and their exceptional electronic transport makes them a suitable substitute for active layers in future nanoelectronic devices.[7–10] Devices based on the hybrid system, combining SWNTs and SLG, have shown great potential in terms of electrical conductivity[11] and mechanical strength,[12] and also have found applications in various fields, such as transparent conducting electrodes,[13,14] active layers in TFTs,[15] humidity and gas sensors,[16] biomedical applications,[17] next generation aromatic compound adsorbents,[18] *etc.* To improve and tune the desired properties for advanced applications such as transparent electrodes and active layers in TFTs, it is very important to understand the structure of SWNT–SLG junction at the atomic scale and various interactions between the two, which modify the properties of the hybrid nanostructures.

The geometrical deformations in SWNTs and bi-layer graphene, due to the interaction between atoms at the junction, have been discussed by W. Ma *et al.*,[19] but only for semiconducting zigzag tubes. In their study, modifications in the shape of supported SWNTs on graphene were observed after the relaxation of the hybrid in terms of unequal horizontal and vertical SWNT diameters and a dip was appeared in graphene. Variations in the electronic structure of SWNTs have previously been reported when in contact with graphene nanoribbons.[20] A few experimental studies have[21–23] addressed the shifts in the Raman mode frequencies of SWNTs and SLG in the hybrid system and it was claimed that the shifts occur as a consequence of charge transfer between the two at the heterojunction. In these studies, the charge transfer between SWNTs and SLG, responsible for the Raman peak shifts, is ascribed to the work-function difference between these structures and any other atomic interaction between the two components is not taken into account. As reported in ref. 24–30, the introduction

[a]*Department of Materials Science and Engineering, Indian Institute of Technology Kanpur, Kanpur 208016, Uttar Pradesh, India. E-mail: agaur@iitk.ac.in*

[b]*Samtel Centre for Display Technologies, Indian Institute of Technology Kanpur, Kanpur 208016, Uttar Pradesh, India*

† Electronic supplementary information (ESI) available: (1) Table showing the structural specifications and the deformation behavior of hybrid nanostructures, (2) Slater–Koster (S–K) parameters in tight-binding DFT, (3) phonon frequencies in hybrid nanostructures studied in this work (data used for plotting Fig. 5), and (4) variation in the phonon frequencies of pristine SWNTs and SLG with charge. See DOI: 10.1039/d0na00881h

of charges (through gate biasing) in SWNTs or SLG causes a shift in the Fermi level and *in situ* Raman measurements show shifts in Raman active vibrational frequencies. A very striking feature of these studies is that for both types of charges (electrons and holes), the prominent peak in the G-band is blue shifted for both SWNTs and SLG, which is also supported by theoretical calculations.[24–26,28,31,32] It has also been reported that strain in the structure of SWNTs and graphene may lead to shifts in their Raman active phonon frequencies.[33–40] We have calculated the relative deformation in the structures of SWNTs and SLG in hybrids with respect to the pristine components (*i.e.* pristine SWNTs and SLG) and illustrated the trend of deformation with changing tube chirality and diameter, though the discussion in ref. 22 dismisses any effect of strain on the Raman mode frequency shifts in hybrid nanostructures.

In this work, we have explored the structural and vibrational properties of SWNT–SLG hybrid nanostructures computationally within the framework of tight-binding DFT in order to understand the nature of interactions at the junction and to delineate the effects of these interactions on the vibrational properties of hybrid nanostructures. These interactions could be the vdW forces between the atoms of SWNTs and SLG, local structural deformations and charge transfer between the two. This paper is organized in the following way: in Section 2, the atomic structures of hybrids of SWNTs and SLG have been discussed and a thorough description of the calculation details for structural optimization and phonon dispersion calculations has been outlined by describing the method and other parameters used to perform the quantum mechanical calculations. Following this, in Section 3, different types of interactions occurring between SWNTs and SLG within hybrid systems are analyzed separately and later, the effect of these interactions on the Raman active phonon mode frequencies of the components has been studied. With this, we have estimated the approximate contribution of different factors to the total observed frequency shift of different modes in SWNT–SLG hybrids. Finally, the conclusions made based on this work are briefly presented in Section 4.

2 Calculation details

2.1 Structural details

The SWNT structures used in this work are generated using TubeGen-3.4 (ref. 41) structure generator. Hybrid nanostructures (with CNT periodicity in the *z*-direction) of SWNT–SLG were constructed by placing both SWNTs and monolayer graphene in the same unit cell at approximate vdW separation (~3 Å of bi-layer graphene) in AB configuration. The width of the graphene unit cell (in *x*-direction) for hybrid nanostructures was chosen such that the SWNTs, placed in the middle of the unit cell, do not interact with each other under periodic boundary conditions, as shown in Fig. 1. An armchair chain of graphene is used to form a periodic hybrid system with armchair tubes (Fig. 1(a) and (b)) and similarly a zigzag graphene chain is combined with zigzag tubes to make a periodic hybrid structure (Fig. 1(c) and (d)). The structural specifications of the different hetero-structures formed are mentioned in

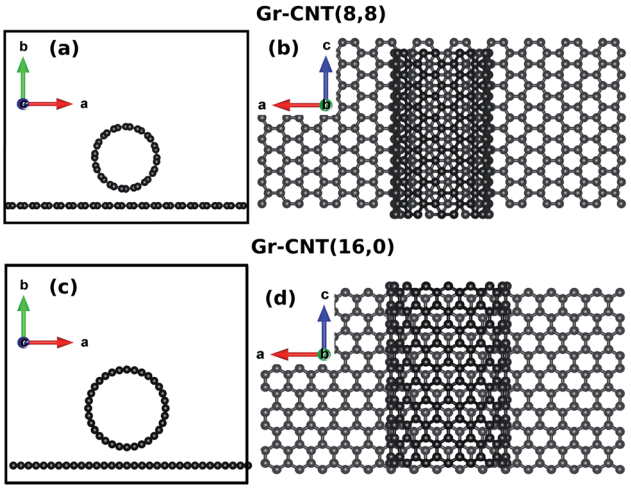

Fig. 1 Hybrid structures of graphene-CNT(8,8) and graphene-CNT(16,0); (a) & (c) show the top view of the hybrids; and (b) & (d) show the front view of hybrid supercell structures, shown for AB-stacked configuration. Visualization software VESTA[42] is used for visualizing the hybrid nanostructures.

Tables 1(a) and (b) in ESI-S.1.† Approximately 20 Å of vacuum is created in the non-periodic direction (perpendicular to the graphene sheet, *i.e.* the *y*-direction) to avoid any interaction with spurious replica images. Out of the wide range of available chiralities, CNT (5,5), (6,6), (7,7), (8,8), (9,9), (10,10) and (11,11) for forming the systems of armchair SWNT–SLG and CNT(8,0), CNT(10,0), CNT(13,0) and CNT(16,0) for making the systems of zigzag SWNT–SLG were chosen.

2.2 Structure optimization and phonon dispersion calculations

We use the density functional based tight binding (DFTB) method implemented in the quantum mechanical simulation software package DFTB+[43,44] (version-18.2) to perform the atomic simulations. This method includes the recent DFTB model DFTB3 (ref. 45), which is based on a third-order Taylor-like expansion of the Kohn–Sham (DFT) total energy with respect to a reference charge density with improved Coulomb interactions between the atomic partial charges. DFT-D3 dispersion correction (method used in the code 'DFTD3' by Stefan Grimme *et al.*[46,47]) is also added to incorporate the vdW correction to the interactions between components in hybrid structures. DFTB has many extensions to the original DFT method and it is also approximately three orders of magnitude faster than DFT. The hybrid structures of SWNT–SLG contain a large number of atoms (*i.e.* 56–128 atoms in the hybrid unit-cell and a supercell consisting of 5 such unit-cells is used for the phonon dispersion calculations) and tight binding DFT methods are most suitable when dealing with such a large number of atoms in a system.

Structures used in this work are relaxed with a self-consistent (SCC) charge tolerance of 10^{-8} until the force on each atom is less than 10^{-6} au (Hartree Bohr^{-1}). The geometry optimization is done by allowing all the atoms and the lattice constants to

move freely for individual components (SWNTs and SLG). The lattice constants are kept fixed for SWNT–graphene hybrids and ionic-relaxation is allowed to minimize forces on all atoms to create relaxed hybrid nanostructures. A dense enough uniform ($2 \times 2 \times 16$) Monkhorst–Pack k-point grid is used for the relevant reciprocal space integration. The electronic temperature is kept at 100 K in these calculations. This temperature was opted to treat metallic systems for better convergence. The variation of total energy and Fermi energy with the electronic temperature is analyzed with no significant changes in the value at 100 K. As reported by T. A. Niehaus *et al.*,[48] out of a number of provided Slater–Koster parameters, 3ob-freq-1-1 Slater–Koster parameters are particularly optimized for the vibrational frequency calculations and we also use the same for structural optimization and phonon dispersion calculations. More details on the Slater–Koster parameters are provided in ESI-S.2.† The phonopy code,[49] interfaced with the DFTB+ code, is used for phonon dispersion calculations with the supercell method. Phonopy generates a number of supercell structures based on the symmetry and size of the primitive unit cell with somewhat displaced atoms (from their equilibrium positions) and later builds the dynamical matrix by evaluating force constants from the forces (as a consequence of the displacement of atoms) calculated by using the DFTB + code for these perturbed structures. The single point force calculations are performed at the Γ-point with a self-consistent charge tolerance of 10^{-8}. Supercell dimensions were kept at $(1 \times 1 \times 5)$ for pristine SWNT and graphene structures; the same was also chosen for the hybrid systems.

3 Results and discussion

3.1 Interaction between SWNTs and graphene

In the unrelaxed state, the hybrid SWNT–graphene structures, as shown in Fig. 1, have large forces acting between some of the atoms of SWNTs and graphene, which are in close proximity to each other. These forces were minimized to form relaxed hybrid structures through ionic relaxation of the unit cells (keeping unit cell dimensions fixed), such that the forces on each atom are below a given cut-off (10^{-6} au). Fig. 2 shows a pictorial representation of forces under un-relaxed (Fig. 2(a) and (c)) and relaxed (Fig. 2(b) and (d)) conditions, acting on each atom in Gr-CNT(8,8) and Gr-CNT(16,0) hybrids. Blue vectors originating from atoms show the relative magnitude of forces. Forces have been rescaled by a factor of 5000 for better visualization. Initially, in the un-relaxed states of hybrids, in Fig. 2(a) and (c), the forces are relatively very high on atoms near the junction. The atoms of SWNTs and graphene at the closest contact repel each other, whereas atoms next to it attract. During the structural relaxation, atoms move in such a way that these forces get minimized and this continues until the forces on each atom are below a given cut-off. Gradually, the SWNTs acquire a shape with an elliptical cross section (similar to the deformation described by W. Ma *et al.*[19]) and graphene develops a curvature around SWNTs in the relaxed geometry (Fig. 2(b) and (d)). The minimum separation between SWNTs and graphene stays close

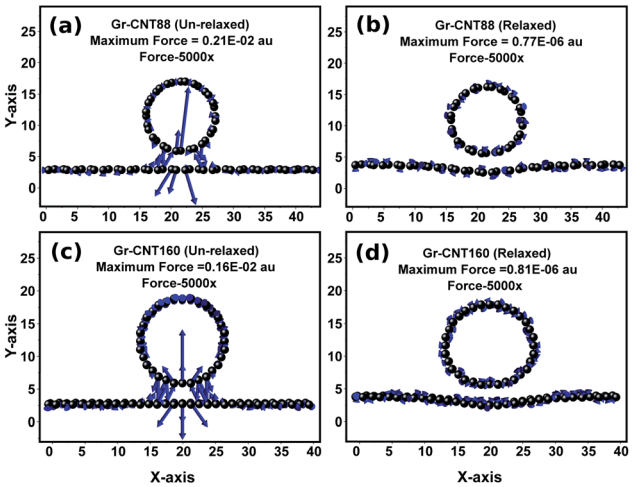

Fig. 2 Illustration of the forces acting on each atom in Gr-CNT(8,8) and Gr-CNT(16,0) in un-relaxed and relaxed hybrid structures. Blue vectors denote the relative magnitude of forces, scaled by a factor of 5000, for the ease of visualization. The maximum force component in each step is also denoted in figures.

to ~3.0 Å (which is our initial separation based on the separation in AB-stacked bilayer graphene) after structural relaxation.

The deformation in relaxed hybrid structures is defined in terms of ΔDx and ΔDy as the difference in horizontal and vertical tube diameters with respect to the un-deformed states for SWNTs and a dip created in graphene within the hybrid. Table-1(b) (ESI-S.1†) summarizes the deformations in the relaxed structure for different hybrids analyzed in this work. The structural symmetry of the SWNTs and graphene is broken in the deformed states. The deformation in SWNTs and graphene are found to be increasing with increasing tube diameter, irrespective of the tube's conductivity (semiconducting or metallic), as shown in Fig. 3.

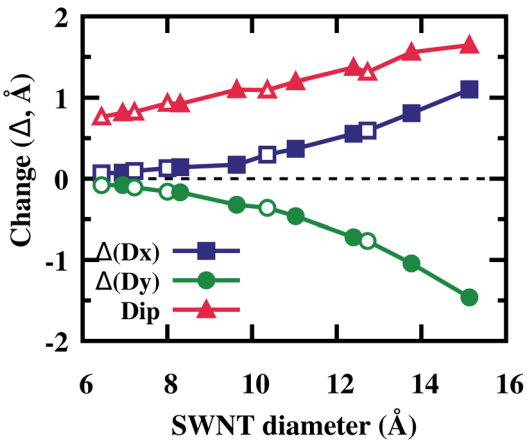

Fig. 3 Structural deformations in SWNTs and SLG in relaxed hybrid structures as a function of SWNT diameter. (ΔD_x) and (ΔD_y) represent the change in SWNT diameters in horizontal and vertical directions respectively and dip represents deformation in graphene [note: filled and open symbols correspond to hybrid structures with armchair and zigzag SWNTs, respectively].

The structural deformations occurring due to the vdW interaction between SWNTs and graphene is larger for larger diameter tubes and the corresponding dip in graphene is also higher. One reason for this behavior could be that the tubes with a larger diameter have a smaller curvature and in turn a greater number of atoms of SWNTs interact with graphene, and hence result in larger deformations (SWNTs) and a higher dip (graphene). Also, SWNTs with a smaller diameter have higher force constants in comparison to the large diameter tubes, which results in stiffer bonds between atoms and makes it difficult to deform the tubes with a small diameter. This can be confirmed from the trend shown in Fig. 3 for SWNT deformations and the dip in graphene as a function of SWNT diameter.

Apart from the structural deformation, interaction between SWNTs and graphene may also be electronic in nature, leading to charge transfer between them in the hybrid structures. Charge distribution in SWNTs and graphene is analyzed within the hybrids for both relaxed and unrelaxed states and it is observed that a few atoms of SWNTs and graphene near the junction area have more charges (positive or negative) in comparison to the initial atomic charges on each atom in pristine states as a result of the charge redistribution. For more clarity, a visual representation of the redistribution of atomic charges in Gr-CNT(8,8) and Gr-CNT(16,0) hybrids with a vdW separation between the components is shown in Fig. 4, for the unrelaxed (4(a) & 4(b)) and relaxed (4(c) & 4(d)) geometries. The red color denotes the presence of positive charges (lack of electrons) and blue represents the negative charges (excess of electrons). From Fig. 4, it is clearly perceptible that atoms near the heterojunction have an excess of electrons/holes and the charge interaction between SWNTs and graphene is localized near the junction area. In this redistribution of charges, the total charge exchanged between SWNTs and graphene are the same but opposite in sign. In Gr-CNT(8,8) and Gr-CNT(16,0) hybrids, a total of 0.0016 and 0.0034 electrons per unit-cell were transferred from graphene to SWNTs respectively.

3.2 Effect of the interaction on Raman mode frequencies

In the previous section, we analyzed different interactions that might occur between SWNTs and graphene in the hybrid system. These interactions are forces (acting on atoms in unrelaxed hybrids), structural deformation (of the components in relaxed hybrids) and electronic interaction (charge transfer) between SWNTs and graphene. We posit that the vibrational modes of SWNTs and graphene within the hybrid structure should be sensitive to these interactions. The effect of these causes on the vibrational properties of SWNTs and SLG individually has been shown in the previous literature (charge: ref. 24–30 and deformation/strain: ref. 33–40) and it is essential to examine how these factors (separately and in combination) affect the vibrational properties of SWNTs and SLG in the hybrid system.

A shift in phonon frequencies can occur only due to the changes in force constants, that is the stiffness of bonds between atoms. If the charges on atoms are modified or the atoms are under forces/strain, the force constants of the bonds will change because of many possible reasons, such as the modified electrostatic interaction between atoms or modified bond lengths, which in turn lead to changes in the corresponding phonon frequencies.[51]

The phonon dispersion curves for pristine components (SWNTs and SLG), unrelaxed and relaxed hybrids and separated deformed components were computed as per the calculation details shared in Section 2.2. The animation of phonon modes at the Γ-point was visualized using v_sim software[52] to identify the phonon mode frequencies corresponding to the radial breathing (RBM), longitudinal optical (LO) and transverse

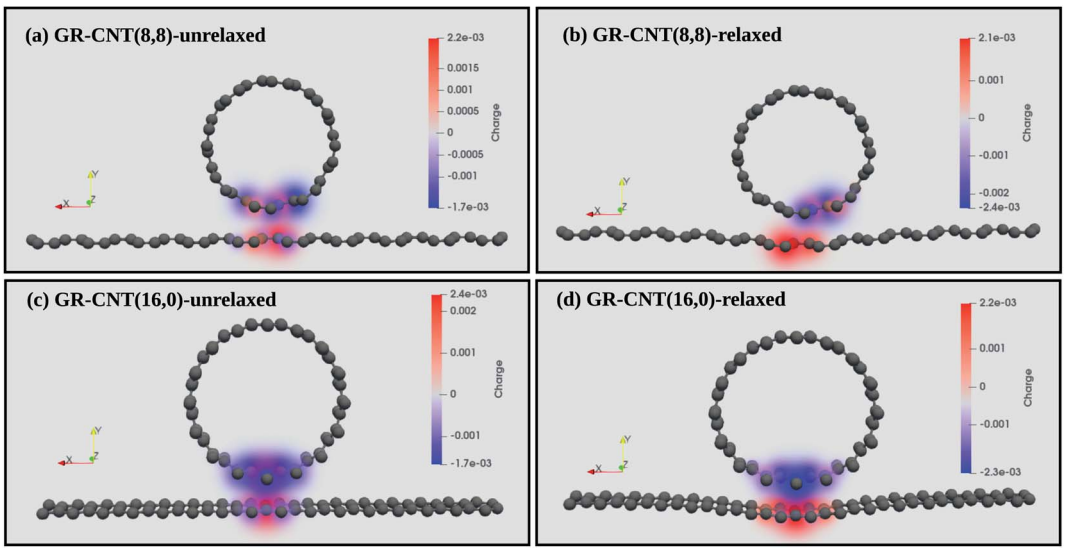

Fig. 4 A visual representation (plotted in a visualization application Paraview[50]) of the redistribution of atomic charges in Gr-CNT(8,8) and Gr-CNT(16,0) in unrelaxed and relaxed hybrid structures, with a 3 Å separation between the components. Red and blue colors stand for holes and electrons respectively.

optical (TO) vibrations of SWNTs and longitudinal optical (LO) and transverse optical (TO) vibrations of SLG. For hybrid structures, the vibration of atoms in components (SWNTs and SLG) was considered separately to identify the phonon modes, which is later verified by calculating the overlap of the eigenvectors of Raman active vibrational modes in pristine SWNTs and graphene (RBM, LO-CNT, TO-CNT, LO-Gr and TO-Gr) with all the modes present in relaxed and unrelaxed hybrid structures and the modes having the maximum overlap are sorted out. The phonon frequencies of pristine components, unrelaxed and relaxed hybrid structures and deformed components for various SWNT–SLG systems are listed in Table 2 in ESI-S.3.† We have also calculated and listed shifts in phonon frequencies with respect to pristine components in Table 2 (ESI-S.3†).

The shift in phonon frequencies for RBM, LO and TO vibrations is plotted (separately for hybrids with armchair and zigzag SWNTs at the vdW separations with graphene) for the unrelaxed and relaxed states of the hybrids and for separated deformed components for a range of tube diameters (hybrid systems described in Section 2.1), as shown in Fig. 5. For unrelaxed hybrid structures, any deviation in the vibrational frequencies of different modes of SWNTs and graphene with respect to the pristine components (SWNTs or graphene) can be ascribed to the presence of vdW forces and/or to the charge transfer between them. Similarly, a variation in the vibrational frequencies in relaxed hybrid structures can be due to structural deformations in individual components and/or due to the charge transfer between them. In separated deformed components, the change can occur due to the structural deformation and/or due to forces acting on atoms. In this section, we have tried to analyze the relative contribution of these factors to the total shift observed in phonon frequencies within a hybrid. By taking into consideration the factors acting in different states, *i.e.* the unrelaxed, relaxed and individual deformed states, the approximate effect of the three factors on hybrid systems can be calculated.

In unrelaxed hybrids, where the effect of vdW forces and charge interaction is considered, insignificant changes

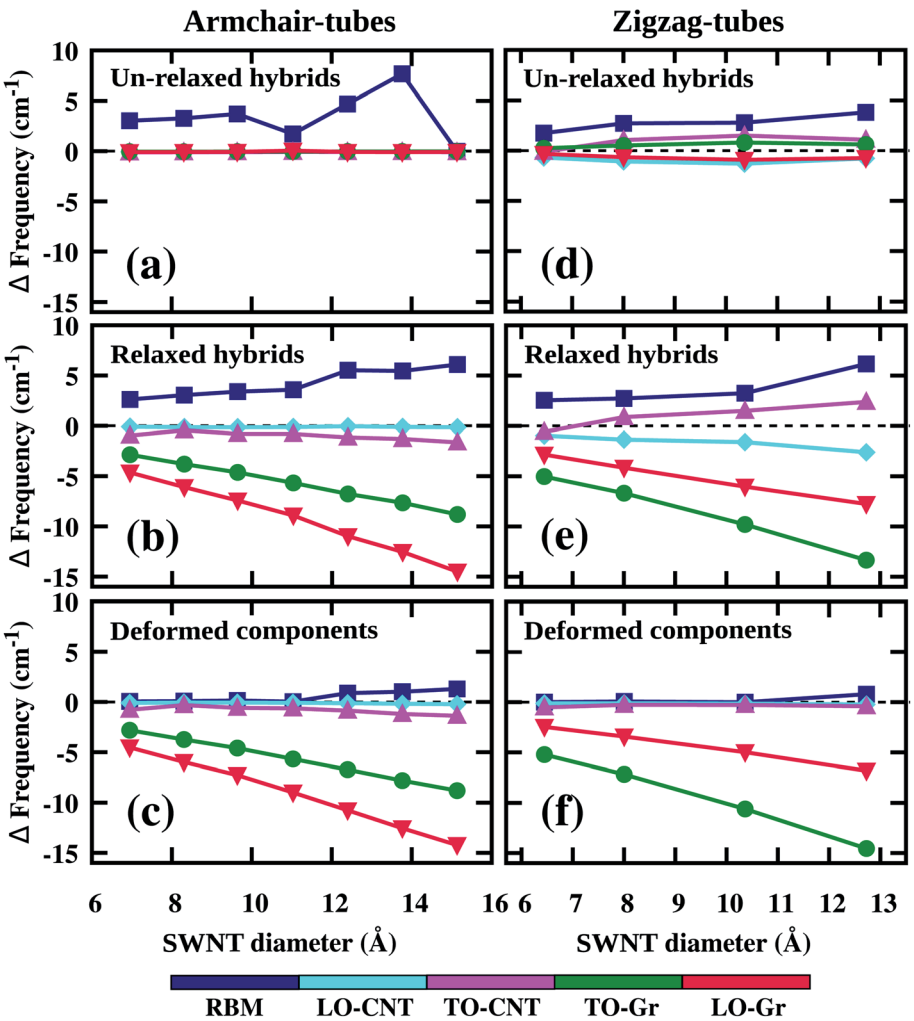

Fig. 5 Variation of the Raman active phonon frequencies (RBM, LO & TO modes) with the SWNT diameter in unrelaxed and relaxed hybrid structures and for deformed individual components calculated separately. Figure (a)–(c) show the variation for armchair (metallic) SWNTs and graphene hybrid structures; and figure (d)–(f) show the same for zigzag (semiconducting) SWNTs and graphene hybrid structures.

(<1 cm^{-1}) are observed in the LO and TO mode frequencies of armchair-SWNTs with respect to the pristine frequencies (Fig. 5(a)). In hybrids with zigzag-SWNTs (Fig. 5(d)), a small shift of ~1 cm^{-1} is observed in the LO–TO mode frequencies but in opposite directions. The effect of charge introduction (both positive and negative) on the vibrational frequencies in isolated SWNTs and graphene has been discussed for the components of one of the hybrid systems with armchair tubes (GR-CNT88) and one with zigzag tubes (GR-CNT160) in the ESI (ESI-S.4†). If we assume that the charges exchanged at the heterojunction are uniformly distributed over all atoms of the SWNT unit, the contribution of transferred charges to the observed change in phonon frequencies can be calculated. The change in the TO & LO mode frequencies of SWNTs due to the charge transfer in the GR-CNT(8,8) hybrid is 0.03 and 0.11 cm−1 and in the GR-CNT(16,0) hybrid, it is 0.34 and −0.01 cm^{-1} respectively (calculated from ESI-S.4, Fig. 1(a) and (c) and Table 3†). It can be seen that the effect of charge interaction on the vibrational mode frequencies of SWNTs (both armchair and zigzag) is very small (<1 cm^{-1}) for the amount of charge transferred at the heterojunction and any change in frequencies <0.1 cm^{-1} can be considered negligible (or "no change" (NC)).[53] From our discussion in ESI-S.4,† in armchair tubes, both LO and TO mode frequencies are upshifted with introduced charges, whereas, in zigzag tubes, the TO mode frequency is upshifted, but the LO mode frequency has a relatively very small downshift. The observed total shift in SWNT LO and TO mode frequencies in zigzag hybrids (Fig. 5(d) and Table 2, ESI-S.3†) are approximately of the same order, which cannot be explained as only due to the charge interaction. So the other interaction, *i.e.* vdW forces, must also be participating in causing the observed shift. The effect of vdW forces on phonon frequencies can simply be calculated by subtracting the change caused by excess charges from the total shift observed in unrelaxed hybrids. In armchair-CNT(8,8), both LO and TO mode frequencies are downshifted by −0.11 and −0.17 cm^{-1} respectively,[53] whereas in zigzag-CNT (16,0), the TO mode is upshifted by 0.75 cm^{-1} and the LO mode is downshifted by −0.77 cm^{-1} due to the effect of vdW forces. It should be noticed here that charge interaction and vdW forces act conversely in the case of armchair tubes, but in zigzag tubes the two factors add up to cause the total shift. Again, the effect of vdW forces on the phonon frequencies of SWNTs (both armchair and zigzag) is very small (<1 cm^{-1}). The frequency change in the TO and LO modes of SWNTs (within hybrids GR-CNT(8,8) and GR-CNT(16,0)) caused by the charge transfer and vdW forces is tabulated in Table 1.

Similarly, in the case of relaxed hybrids (Fig. 5(b) and (e)), where the charge interaction and structural deformation affect the phonon frequencies, the contribution of these factors to the total observed frequency shift in components is shown in Table 1. In armchair-SWNTs, the LO mode frequencies show a negligible downshift and the TO frequencies show a small downshift, whereas in zigzag-SWNTs, the TO mode frequencies upshift, but the LO mode frequencies downshift by approximately the same amount, as shown in Fig. 5(b) and (e). The effect of charge transfer is calculated in the same way as our discussion in ESI-S.4.† The effect of structural deformations in components is calculated by subtracting the change caused due to introduced charges from the total observed frequency shift. From Table 1, similar to the observations for vdW forces in unrelaxed hybrids, structural deformation affects the phonon frequencies conversely to the charge interaction in armchair tubes, but the effects add up in the case of zigzag tubes. The contribution of deformations to the changes in TO & LO mode frequencies in armchair-CNT(8,8) and zigzag-CNT(16,0) in relaxed hybrids is −0.86 and −0.32, and 1.72 and −2.60 cm^{-1} respectively.[53] The compressive deformation downshifts the LO and TO mode frequencies in armchair-SWNTs, where the TO vibrations are affected more than the LO vibrations, whereas in zigzag-SWNTs, the deformation has contrasting effects on the TO and LO mode frequencies affecting the LO vibrations more.

Table 1 Contribution of different factors to the total observed change in the phonon frequencies of components in GR-CNT(8,8) and GR-CNT(16,0) hybrids [note: here "NC" implies negligible or no change (<0.1 cm^{-1})]

		Effect of factors (cm^{-1})			
		Charge			
Hybrid system	Phonon modes	(Unrelaxed hybrid)	(Relaxed hybrid)	vdW force (unrelaxed hybrid)	Deformation (relaxed hybrid)
GR-CNT(8,8)					
CNT(8,8)	RBM	NC	NC	**1.71**	**3.57**
	TO	NC	NC	−0.11	−0.86
	LO	0.11	0.19	−0.17	−0.32
Graphene	TO	0.10	0.13	−0.12	**−5.80**
	LO	NC	NC	NC	**−8.92**
GR-CNT(16,0)					
CNT(16,0)	RBM	NC	NC	**3.81**	**6.16**
	TO	0.34	0.66	0.75	1.72
	LO	NC	NC	−0.77	−2.60
Graphene	TO	0.33	0.63	0.29	**−13.98**
	LO	NC	NC	−0.71	**−7.70**

Phonon calculations on separated deformed SWNTs (Fig. 5(c) and (f)) (*i.e.* excluding graphene atoms from the relaxed hybrid unit-cell) will have the combined effect of deformation and forces on vibrational frequencies. It should be noted that atoms within the deformed structures will have appreciable forces and the direction of forces in deformed SWNTs and graphene is inverted from the direction in unrelaxed hybrids, which may also cause shifts in Raman vibrational mode frequencies.

We can summarize these observations as follows: the changes in phonon mode frequencies have a combined effect of different factors, where these factors affect different vibrational modes differently and may cause Raman mode frequency shifts in opposite directions. The contribution of various factors to the observed total change in the phonon frequencies of components can be deconvoluted in the above mentioned way, but the frequency shift observed in the LO & TO modes of SWNTs is very small in both the states of hybrids, which indicates that the

charge exchanged at the junction, the vdW forces and the extent of structural deformations are very small to cause a noticeable change in the LO–TO phonon frequencies of SWNTs at the vdW separation from graphene. However, a significant increase has been observed in the RBM frequencies as an effect of the vdW interaction and radial deformation in unrelaxed and relaxed hybrids (Fig. 5(a), (b), (d) and (e) and Table 1), which is consistent with previously reported results.[33–38] The effect of charge transfer occurring at the heterojunction has a negligible effect on the RBM frequencies (as discussed in our calculation of the phonon frequency variation with introduced charges in ESI-S.4†).

On the other hand, the frequency shifts observed in graphene phonon modes within the hybrids are more significant. Both LO and TO modes are down-shifted from their pristine values and also show a dependence on the tube diameter. The frequency shift (down-shift) increases with increasing deformation in graphene (increasing tube diameter) (Fig. 5(b), (e), (c) and (f)). It has been reported previously[39] that graphene Raman mode frequencies down shift with increasing strain and the splitting between LO and TO frequencies also increases with increasing strain.[40] Analysis similar to that done above for SWNTs has been performed for graphene. From the analysis, it has been observed that the effect of charge transfer and vdW forces on graphene phonon frequencies is similar to the case of SWNTs, but it is negligible in comparison to the frequency shift caused by structural deformations (as shown in Table 1), which is a simple manifestation of the introduced curvature in graphene at the heterojunction. A frequency downshift of −5.80 and −8.92 cm^{-1} to the TO and LO modes of graphene in the GR-CNT(8,8) hybrid and −13.98 and −7.70 cm^{-1} in the GR-CNT(16,0) hybrid is contributed by structural deformations. The effect of charge interaction and vdW forces is experienced by only a small fraction of atoms in the graphene unit cell. So, the frequency shifts occurring in graphene are mainly deformation induced.

The discussion above on the phonon frequencies in hybrid systems of SWNT–graphene suggests that the frequency shift observed in SWNTs and graphene is not only charge interaction induced. Other interactions, such as vdW forces at the heterojunction and deformation in component structures, also play a role, with structural deformation being the leading cause of Raman mode frequency shifts. However, it should be noted that structural deformations in the hybrid nanostructures of SWNTs and SLG under experimental conditions have not been reported to the best of our knowledge and we suggest that this may be explored further experimentally.

From our calculations, it is observed that the charge transfer occurring between SWNTs and SLG at 3.0 Å separations is very small and does not cause any significant shift in the vibrational frequencies of either SWNTs or SLG. With decreasing separation, the charge transfer between SWNTs and SLG increases, as shown in Fig. 6. Fig. 6 illustrates the total charge (electrons) transferred to SWNTs at varying separation from graphene. The maximum charge transfer takes place at ∼2.1 Å. The same amount of total charge is been removed from graphene. The inset of Fig. 6 is a visual representation of the charge transfer in

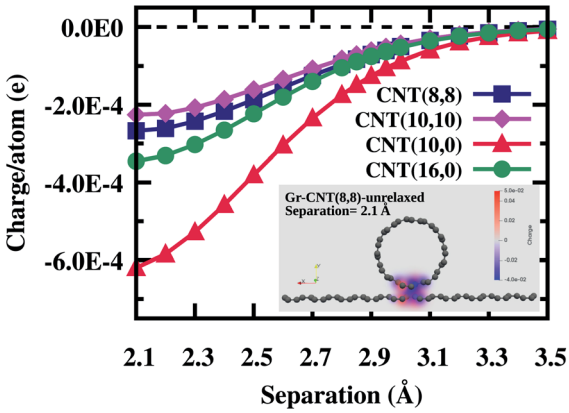

Fig. 6 Charge per atom on SWNTs at varying separation from graphene for Gr-CNT(8,8), Gr-CNT(10,10), Gr-CNT(10,0) and Gr-CNT(16,0) hybrid structures. Note: negative charge indicates an excess of electrons. The inset shows the visual representation of atomic charges at a 2.1 Å separation in the GR-CNT(8,8) unrelaxed hybrid structure.

the Gr-CNT(8,8) hybrid at a 2.1 Å SWNT-Gr separation. The vdW interaction between SWNTs and SLG also increases with decreasing separation, which results in larger forces between atoms in unrelaxed hybrids. In relaxed hybrids with less initial separations, the equilibrium separation approaches 3.0 Å after relaxation, resulting in similar deformed hybrid structures to those with 3.0 Å initial separations.

The normalized change (with respect to the value at the vdW separation) in the total transferred charge and the average force on atoms with decreasing separation between SWNTs and graphene is shown for different hybrids in Fig. 7. The forces acting between the atoms of SWNTs and graphene increase rapidly in comparison with the charge transferred between SWNTs and graphene. This suggests that at smaller separations, the effect of forces on the phonon frequencies of SWNTs and graphene will be much higher in comparison to the effect of charge introduced at the heterojunction. For example in zigzag-CNT(10,0),

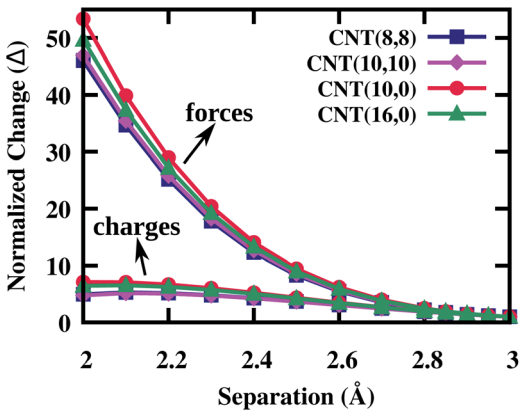

Fig. 7 Normalized change in the total transferred charge and average force on SNWTs for Gr-CNT(8,8), Gr-CNT(10,10), Gr-CNT(10,0) and Gr-CNT(16,0) hybrid structures as a function of separation from SLG. Normalization of values is done with respect to the value at the vdW separation (∼3 Å).

at a 2.5 Å separation, the observed shift in RBM, LO and TO mode frequencies is 16.09, −5.54 and 6.86 cm^{-1} respectively (compared to the shifts at 3.0 Å, which are 2.72, −1.08 and 1.05 cm^{-1} respectively (Table 2 in ESI-S.3†)). From our discussion of the phonon frequency variation with charges in ESI-S.4,† this downshift in LO mode frequency cannot be explained as the effect of only charge transfer, even if we consider the upper limit, *i.e.* if we assume all the atoms of SWNTs to have the maximum charge transferred at the heterojunction. So, even at smaller separations, the observed shift in the phonon mode frequencies of SWNTs and graphene within the hybrids is not caused only due to the charge exchanged at the heterojunction, but the other factors, *i.e.* the forces acting between atoms and the deformations in the component structures are also needed to be considered for causing the resultant Raman frequency shifts.

4 Conclusions

In this work, we have calculated the effect of various interactions between the atoms of single-layer graphene (SLG) and single wall carbon nanotubes (SWNTs) computationally within the framework of tight binding DFT approximation in order to study the structural and vibrational properties of SLG–SWNT nano-structure hybrids. Our calculations show that the vdW forces between the atoms of the two components (SWNTs and SLG), when separated by 3.0 Å, lead to structural deformations in SLG and SWNTs to minimize these forces. Phonon calculations and the comparison of Raman active modes in pristine components (SLG and SWNTs), un-relaxed and relaxed hybrids, and deformed separated components allow us to deconvolute the effect of charge transfer, forces and structural deformations on Raman mode frequencies in hybrid nanostructures. The charge transfer due to interaction between the atoms of SLG and SWNTs is highly localized and is not sufficient to cause appreciable shifts in the in-plane Raman active modes (*i.e.* the LO and TO modes of the G-band) of SLG and SWNTs. However, structural deformations cause shifts in Raman mode frequencies to a small extent (<2 cm^{-1}) in SWNTs and to a significant extent (up to 15 cm^{-1}) in SLG. The amount of charge transfer increases if the separation between the components is decreased, which also leads to an increase in forces acting on the atoms of SWNTs and SLG at the junction. Overall, our calculations suggest that while analyzing the Raman spectra of such hybrid nanostructures, careful attention should be given to all possible factors that might cause changes in Raman active mode frequencies and experiments could be designed to study the effect of individual factors.

Conflicts of interest

There are no conflicts to declare.

Acknowledgements

The authors would like to acknowledge support from HPC, IIT Kanpur for the use of their computing facility in the present work. J. Srivastava acknowledges financial support from MHRD, Govt of India and A. Gaur acknowledges support from MeitY, Govt of India under the Visvesvaraya YFRF program (MEITY-PHD-896).

References

1 R. Saito, G. Dresselhaus and M. S. Dresselhaus, *Physical Properties of Carbon Nanotubes*, Imperial College Press And Distributed By World Scientific Publishing Co, 1998.
2 H. F. Bettinger, *ChemPhysChem*, 2004, **5**, 1914–1915.
3 P. Avouris, M. Freitag and V. Perebeinos, *Nat. Photonics*, 2008, **2**, 341–350.
4 J. A. Misewich, R. Martel, P. Avouris, J. C. Tsang, S. Heinze and J. Tersoff, *Science*, 2003, **300**, 783–786.
5 K. S. Novoselov, A. K. Geim, S. V. Morozov, D. Jiang, Y. Zhang, S. V. Dubonos, I. V. Grigorieva and A. A. Firsov, *Science*, 2004, **306**, 666–669.
6 A. Geim and K. Novoselov, *Nat. Mater.*, 2007, **6**, 183–191.
7 S. J. Tans, A. R. M. Verschueren and C. Dekker, *Nature*, 1998, **393**, 49–52.
8 P. Avouris, Z. Chen and V. Perebeinos, *Nat. Nanotechnol.*, 2007, **2**, 605–615.
9 D.-M. Sun, C. Liu, W.-C. Ren and H.-M. Cheng, *Small*, 2013, **9**, 1188–1205.
10 B.-J. Kim and J.-S. Park, *Carbon Nanotubes*, IntechOpen, Rijeka, 2018, ch. 11.
11 Y. Liao, K. Mustonen, S. Tulić, V. Skákalová, S. A. Khan, P. Laiho, Q. Zhang, C. Li, M. R. A. Monazam, J. Kotakoski, H. Lipsanen and E. I. Kauppinen, *ACS Nano*, 2019, **13**, 11522–11529.
12 K. Xia, H. Zhan and Y. Gu, *Procedia IUTAM*, 2017, **21**, 94–101.
13 J. Zhang, Z. Chen, X. Xu, W. Liao and L. Yang, *RSC Adv.*, 2017, **7**, 52555–52560.
14 S. H. Kim, W. Song, M. W. Jung, M.-A. Kang, K. Kim, S.-J. Chang, S. S. Lee, J. Lim, J. Hwang, S. Myung and K.-S. An, *Adv. Mater.*, 2014, **26**, 4247–4252.
15 Z. Peng, A. L. Ng, H. Kwon, P. Wang, C.-F. Chen, C. S. Lee and Y. Wang, *Carbon*, 2017, **125**, 49–55.
16 B. Cai, H. Yin, T. Huo, J. Ma, Z. Di, M. Li, N. Hu, Z. Yang, Y. Zhang and Y. Su, *J. Mater. Chem. C*, 2020, **8**, 3386–3394.
17 D. Patel, Y.-R. Seo and K.-T. Lim, *Stem Cells Int.*, 2019, **2019**, 9831853, 18 pages.
18 A. Dichiara, T. Sherwood, J. Benton-Smith, J. Wilson, S. Weinstein and R. Rogers, *Nanoscale*, 2014, **6**(12), 6322–6327.
19 W. Ma and G. Zhang, *Jpn. J. Appl. Phys.*, 2013, **52**, 035101.
20 C. Lee, S. Chen, C. Yang, W. Su and M. Lin, *Comput. Phys. Commun.*, 2011, **182**, 68–70.
21 Y. Liu, F. Wang, Y. Liu, X. Wang, Y. Xu and R. Zhang, *Nanoscale*, 2016, **8**, 12883–12886.
22 G. L. C. Paulus, Q. H. Wang, Z. W. Ulissi, T. P. McNicholas, A. Vijayaraghavan, C.-J. Shih, Z. Jin and M. S. Strano, *Small*, 2013, **9**, 1954–1963.
23 R. Rao, N. Pierce and A. Dasgupta, *Appl. Phys. Lett.*, 2014, **105**, 073115.

24 A. Das, A. K. Sood, A. Govindaraj, A. M. Saitta, M. Lazzeri, F. Mauri and C. N. R. Rao, *Phys. Rev. Lett.*, 2007, **99**, 136803.
25 A. Das, S. Pisana, B. Chakraborty, S. Piscanec, S. Saha, U. Waghmare, K. Novoselov, H. Krishnamurthy, A. Geim, A. Ferrari and A. Sood, *Nat. Nanotechnol.*, 2008, **3**, 210–215.
26 H. Farhat, H. Son, G. G. Samsonidze, S. Reich, M. S. Dresselhaus and J. Kong, *Phys. Rev. Lett.*, 2007, **99**, 145506.
27 K. T. Nguyen, A. Gaur and M. Shim, *Phys. Rev. Lett.*, 2007, **98**, 145504.
28 H. Farhat, K. Sasaki, M. Kalbac, M. Hofmann, R. Saito, M. S. Dresselhaus and J. Kong, *Phys. Rev. Lett.*, 2009, **102**, 126804.
29 A. Das and A. K. Sood, *Phys. Rev. B*, 2009, **79**, 235429.
30 S. Grimm, S. P. Schießl, Y. Zakharko, M. Rother, M. Brohmann and J. Zaumseil, *Carbon*, 2017, **118**, 261–267.
31 S. Pisana, M. Lazzeri, C. Casiraghi, K. Novoselov, A. Geim, A. Ferrari and F. Mauri, *Nat. Mater.*, 2007, **6**, 198–201.
32 N. Caudal, A. M. Saitta, M. Lazzeri and F. Mauri, *Phys. Rev. B*, 2007, **75**, 115423.
33 Z. Liu, J. Zhang and B. Gao, *Chem. Commun.*, 2009, 6902–6918.
34 M. J. Peters, L. E. McNeil, J. P. Lu and D. Kahn, *Phys. Rev. B*, 2000, **61**, 5939–5944.
35 J. Sandler, M. S. P. Shaffer, A. H. Windle, M. P. Halsall, M. A. Montes-Morán, C. A. Cooper and R. J. Young, *Phys. Rev. B*, 2003, **67**, 035417.
36 W. Yang, R. Z. Wang, X. M. Song, B. Wang and H. Yan, *Phys. Rev. B: Condens. Matter Mater. Phys.*, 2007, **75**, 045425.
37 P. Teredesai, A. Sood, S. Sharma, S. Karmakar, S. Sikka, A. Govindaraj and C. Rao, *Phys. Status Solidi B*, 2001, **223**, 479–487.
38 K. Sood, P. V. Teresdesai, D. V. S. Muthu, R. Sen, A. Govindaraj and C. N. R. Rao, *Phys. Status Solidi B*, 1999, **215**, 393–401.
39 Z. H. Ni, T. Yu, Y. H. Lu, Y. Y. Wang, Y. P. Feng and Z. X. Shen, *ACS Nano*, 2009, **3**, 483.
40 T. M. G. Mohiuddin, A. Lombardo, R. R. Nair, A. Bonetti, G. Savini, R. Jalil, N. Bonini, D. M. Basko, C. Galiotis, N. Marzari, K. S. Novoselov, A. K. Geim and A. C. Ferrari, *Phys. Rev. B*, 2009, **79**, 205433.
41 J. T. Frey and D. J. Doren, *TubeGen 3.4, Web-Interface*, 2011.
42 K. Momma and F. Izumi, *J. Appl. Crystallogr.*, 2011, **44**, 1272–1276.
43 B. Aradi, B. Hourahine and T. Frauenheim, *J. Phys. Chem. A*, 2007, **111**, 5678–5684.
44 B. Hourahine, B. Aradi, V. Blum, F. Bonafé, A. Buccheri, C. Camacho, C. Cevallos, M. Y. Deshaye, T. Dumitrică, A. Dominguez, S. Ehlert, M. Elstner, T. van der Heide, J. Hermann, S. Irle, J. J. Kranz, C. Köhler, T. Kowalczyk, T. Kubař, I. S. Lee, V. Lutsker, R. J. Maurer, S. K. Min, I. Mitchell, C. Negre, T. A. Niehaus, A. M. N. Niklasson, A. J. Page, A. Pecchia, G. Penazzi, M. P. Persson, J. Řezáč, C. G. Sánchez, M. Sternberg, M. Stöhr, F. Stuckenberg, A. Tkatchenko, V. W.-z. Yu and T. Frauenheim, *J. Chem. Phys.*, 2020, **152**, 124101.
45 M. Gaus, Q. Cui and M. Elstner, *J. Chem. Theory Comput.*, 2011, **7**, 931–948.
46 S. Grimme, J. Antony, S. Ehrlich and H. Krieg, *J. Chem. Phys.*, 2010, **132**, 154104.
47 S. Grimme, S. Ehrlich and L. Goerigk, *J. Comput. Chem.*, 2011, **32**, 1456–1465.
48 T. A. Niehaus, S. T. A. G. Melissen, B. Aradi and S. M. V. Allaei, *J. Phys.: Condens. Matter*, 2019, **31**, 395901.
49 A. Togo and I. Tanaka, *Scr. Mater.*, 2015, **108**, 1–5.
50 J. Ahrens, B. Geveci and C. Law, *Visualization Handbook*, 2005.
51 W. Yang, R.-Z. Wang and H. Yan, *Phys. Rev. B*, 2008, **77**, 195440.
52 L. Billard, D. Caliste, D. Olivier, A. Lherbier, B. Jérémy, P. Simon, T. Jourdan and Y. Ratao, *V_sim*, http://www.mem-lab.fr/en/Pages/L_SIM/Softwares/V_Sim.aspx.
53 We have considered any change in the phonon frequencies > 0.1 cm^{-1} as an actual effect of interactions between the atoms of graphene and SWNTs (and any shift <0.1 cm^{-1} is considered negligible even though it might be due to actual interactions). To check the extent of shift in phonon frequencies as an effect of forces, we relaxed one system (SWNT-16,0) to a lower force threshold *i.e.*, 1×10^{-3} au (Hartree $Bohr^{-1}$). The changes in the phonon frequencies of different modes (RBM, TO and LO) for this system were found to be in the range of 0.1 $cm^{-1} < \Delta < 1$ cm^{-1} compared to the same system relaxed up to a 1×10^{-6} au force threshold. Hence, we can say that the small frequency shifts (> 0.1 cm^{-1}) presented here represent the actual effect of forces due to various interactions between graphene and SWNTs. The maximum force on atoms in unrelaxed hybrid structures and deformed individual components is also of the order of 1×10^{-3} au (as shown in Fig. 2). These small frequency shifts (up to 0.1 cm^{-1}) are included in the text and Table 1 as a comparison between the effects of various interactions (*i.e.*, the vdW forces, charge transfer and structural deformations).